Article

Climate Change and CO_2 Fertilization Have Played Important Roles in the Recent Decadal Vegetation Greening Trend on the Chinese Loess Plateau

Zhongen Niu [1,*], Honglin He [2], Pengtao Yu [3], Stephen Sitch [4], Ying Zhao [1], Yanhui Wang [3], Atul K. Jain [5], Nicolas Vuichard [6] and Bingcheng Si [1]

[1] School of Resources and Environmental Engineering, Ludong University, Yantai 264025, China
[2] Key Laboratory of Ecosystem Network Observation and Modeling, Institute of Geographic Sciences and Natural Resources Research, Chinese Academy of Sciences, Beijing 100101, China
[3] Ecology and Nature Conservation Institute, Chinese Academy of Forestry, Beijing 100091, China
[4] Faculty of Environment, Science and Economy, University of Exeter, Exeter EX4 4QF, UK
[5] Department of Atmospheric Sciences, University of Illinois, Urbana, IL 61821, USA
[6] Laboratoire des Sciences du Climat et de l'Environnement, LSCE/IPSL, CEA-CNRS-UVSQ, Université Paris-Saclay, F-91198 Gif-sur-Yvette, France
[*] Correspondence: niuzhongen@ldu.edu.cn

Abstract: Vegetation greening has been widely occurring on the Chinese Loess Plateau, and the contributions of human land-use management have been well-understood. However, the influences of climatic change and CO_2 fertilization on reported vegetation variations remain difficult to determine. Therefore, we quantified the impacts of multiple factors on vegetation changes for the Chinese Loess Plateau from 2000 to 2019 by integrating satellite-based leaf area index (LAI) and simulated LAI from dynamic global vegetation models. More than 96% of the vegetated areas of the Loess Plateau exhibited greening trends, with an annually averaged satellite-based LAI rate of 0.037 ± 0.006 m^2 m^{-2} a^{-1} ($P < 0.01$). Human land-use management and environmental change have jointly accelerated vegetation growth, explaining 54% and 46% of the overall greening trend, respectively. CO_2 fertilization and climate change explain 55% and 45% of the greening trend due to environmental change, respectively; solar radiation and precipitation were the main driving factors for climate-induced vegetation greenness ($P < 0.05$). Spatially, the eastern part of the Loess Plateau was dominated by CO_2 fertilization, while the western part was mainly affected by climate change. Furthermore, solar radiation was the key limiting factor affecting LAI variations in the relatively humid area, while precipitation was the major influencing factor in relatively arid areas. This study highlights the important roles that climate change and CO_2 fertilization have played in vegetation greenness in recent decades of the Loess Plateau, despite strong influences of anthropogenic footprint.

Keywords: greening; human land-use management; climate change; CO_2 fertilization; Loess Plateau

1. Introduction

Satellite-based data have revealed increasing greenness across terrestrial ecosystems since 2000 [1,2]. Vegetation changes are closely associated with variations in the carbon budget and ecohydrological processes. The rate and scale of projected climate changes and anthropogenic disturbances in the 21st century have already profoundly impacted terrestrial ecosystems and will continue to do so [3]. To better formulate climate change adaptation and coping strategies, an in-depth understanding of the drivers of vegetation dynamics is required [4]. However, how much multiple environmental factors affect vegetation variations in the context of intense anthropogenic activities has not been clearly quantified.

Environmental change and human land-use management are thought to alter vegetation growth directly or indirectly. First, it has been shown that warming promotes the greening of vegetation at high latitudes [5] by boosting metabolism and extending

the growing season [6], but these positive influences appear to have diminished in the past decade [7,8]. Second, precipitation dominates vegetation greening and browning in water-limited ecosystems [9,10]. Third, increasing CO_2 concentrations in the atmosphere enhances vegetation growth through promoted leaf photosynthesis [11,12]. Globally, dynamic vegetation models and satellite-observed data have suggested that CO_2 fertilization dominates the vegetation restoration processes [13]. Finally, human land-use management is also an important driver of vegetation restoration, as more than 1/3 of vegetation growth at the global scale can be attributed to human land-use management [14,15]. Overall, vegetation growth is affected by various environmental and human factors.

Studies have tried to separate the effects of climate change and anthropogenic activities on vegetation growth [16–20]. The residual method is a commonly used method, which is based on linear regression and is simple to operate [18,21], but it usually ignores the nonlinear effects of climate change on vegetation, leading to large uncertainties in the assessment results. Machine learning methods can overcome these deficiencies, but they lack a clear mechanism [16]. For example, machine learning methods have difficulty disentangling the influences of CO_2 fertilization and climatic change. Therefore, to better understand the driving factors of vegetation change, it is necessary to improve the quantification method using process-based vegetation models.

LAI is a clear physical attribute and can reflect the change in vegetation growth, meanwhile LAI is not only a state variable of process-based models, but also can be retrieved from remote sensing data [1]. Integrated satellite-based LAI and simulated LAI derived from terrestrial biosphere process-based models were used previously to discern natural and human impacts on vegetation variation [2]. Moreover, process-based models allow quantitative separation of the drivers of vegetation change using factorial experiments [13,22,23]. Therefore, the integration of remote sensing vegetation index and process-based model simulation results can deepen our understanding of the driving forces of vegetation change.

The Loess Plateau is an ecologically fragile region that has experienced destruction and restoration processes due to the joint effects of environmental change and human land-use management [24,25]. Increasing precipitation has significantly promoted vegetation restoration; anthropogenic activities such as ecological projects, cropland irrigation, and urban expansion have also significantly altered vegetation growth in the Loess Plateau [24,26]. Several studies have tried to separate the effects of various environmental factors on vegetation growth and the contributions of human land-use management [24,27–29]; however, the influences of climatic change and CO_2 fertilization on reported vegetation variations remain difficult to determine in the Loess Plateau. Therefore, this study aims to: (1) investigate the spatial-temporal dynamics of vegetation variation on the Loess Plateau from 2000 to 2019; (2) quantitatively separate the influences of environmental and anthropogenic factors on vegetation growth; (3) and identify the relative contribution of CO_2 fertilization and climate change on environmentally induced vegetation variation.

2. Materials and Methods

2.1. Study Area

The Loess Plateau is located in northern China and covers 7 provinces (Figure 1). The region belongs to the semi-arid continental monsoon zone, with a multiyear average temperature between 4 °C and 14 °C, and cumulative precipitation between 50 mm and 700 mm. The Loess Plateau has experienced destruction and then restoration processes due to natural and anthropogenic factors [30].
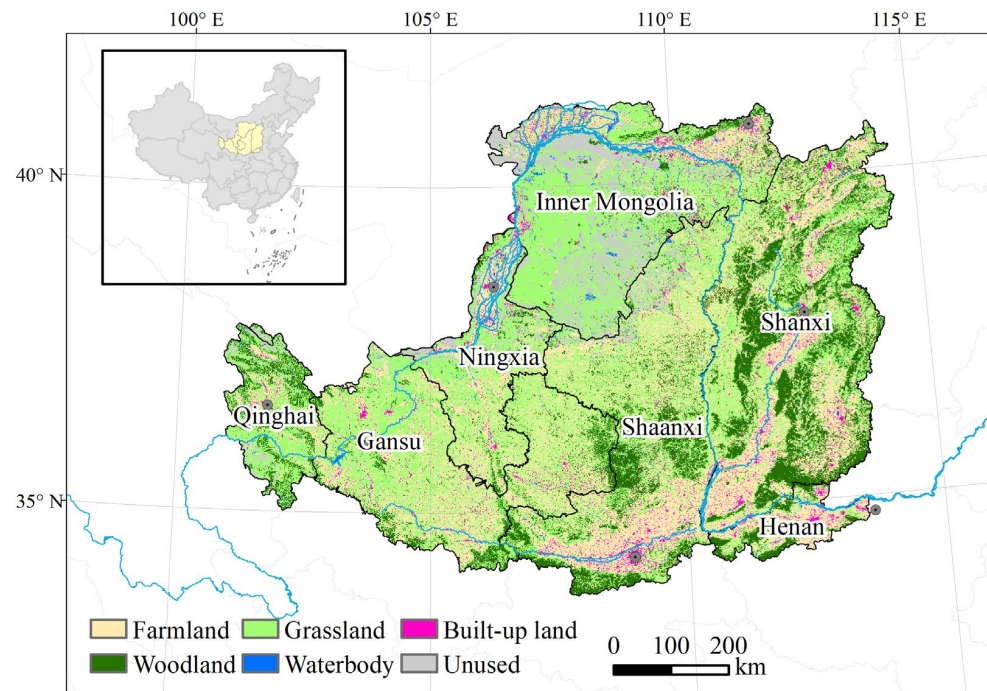
Figure 1. The location and land cover of Loess Plateau in 2015.

2.2. Data and Preprocessing

2.2.1. Satellite-Based LAI

The satellite-based LAI acquired from the MOD15A2H product was used to reflect the actual vegetation. The spatial resolution of MODIS LAI is 500 m × 500 m, and temporal resolution is 8 days. The average value of LAI over the growing season (June–August) was calculated to represent actual vegetation growth variations from 2000 to 2019.

2.2.2. Simulated LAI

The simulated LAI acquired from the TRENDY v9 project (https://blogs.exeter.ac.uk/trendy/, accessed on 1 July 2022) was used to assess the vegetation variations caused by environmental change. Five dynamic global vegetation models (i.e., ISAM, LPJ-GUESS, LPX-Bern, ORCHIDEEv3, and VISIT) with a relatively high spatial resolution of 0.5° × 0.5° was used.

The TRENDY project conducted three simulation scenarios to separate the impacts of different environmental factors on ecosystems. The simulation scenarios "S1" and "S2" were used in this study. For scenario "S1", only atmospheric CO_2 concentration was allowed to vary during the study period; for scenario "S2", both atmospheric CO_2 concentration and climate factors were allowed to change over time. Models incorporating the nitrogen cycle included temporal variations for both the S1 and S2 scenarios. For scenario "S3", land use was also allowed to change. The Land-Use Harmonization (LUH2) product was the dominant land use and cover change driving the data used in scenario "S3". The LUH2 product was constructed from national agricultural land area data, but was not constrained by forest area [31]. The LUH2 product showed a spurious temporal signal of an abrupt increase in cropland area in China since the 1980 s and underestimated the newly established forest area from 1990 to 2019 [32]. Therefore, the LUH2 product was not used to analyze the impact of forest area, and the simulation result of scenario "S3" was not used in this study.

2.2.3. Anthropogenic Factors

To analyze the correlation between the LAI and forest area, data related to forest area were collected from the national forest resource inventory (NFRI) for each province. The

6th, 7th, 8th, and 9th NFRIs covered the periods from 1999 to 2003, 2004 to 2008, 2009 to 2013, and 2014 to 2018, respectively. Meanwhile, a newly developed historical land cover database [32] for China was used to reflect the vegetation coverage rate. The new data incorporate land conversion signals from satellite images, field surveys, and report data; the data can more accurately reflect land-use changes [32]. Additionally, based on the gross domestic product (GDP) dataset, a key indicator of socioeconomic activities, we analyzed the correlations between economic development and vegetation variations.

2.2.4. Meteorological Data

The models in the TRENDY project were driven using either monthly Climatic Research Unit (CRU) [33] or 6 hourly CRU-Japanese 55-year Reanalysis (CRU-JRA55) [34] dataset. The CRU-JRA55 was generated based on the JRA-55 [35] and CRU TS datasets. Temperature, downward solar radiation, specific humidity, and precipitation in JRA-55 were aligned to the meteorological data in CRU TS (4.03). The other variables (e.g., atmospheric pressure, downward long-wave radiation, and wind speed) were not modified. The spatial resolution of CRU data was $0.5° \times 0.5°$.

Additionally, temperature, precipitation, and downward solar radiation from the CRU dataset were used to analyze the influencing factors of LAI.

2.3. Methods
2.3.1. LAI Normalization

The magnitudes of the satellite-based and simulated LAI values differed significantly. To enable comparison of different LAIs, we normalized the LAIs. The normalized LAIs were dimensionless but can capture the interannual percent change in origin satellite-observed and simulated LAIs, which is the focus of this study.

The normalized MODIS LAI ($LAI_{MODIS\_normalized}$) can be obtained by dividing the annual satellite-based LAI by the multi-year average satellite-based LAI:

$$LAI_{MODIS\_normalized,year} = \frac{LAI_{MODIS,year}}{\overline{LAI_{MODIS}}}, \tag{1}$$

where $LAI_{MODIS\_normalized,year}$ and $LAI_{MODIS,year}$ represent the normalized and observed LAI at a certain year (year = 2000, 2001, 2002, ..., 2019), respectively. ($\overline{LAI_{MODIS}}$) represents the multi-year average satellite-based LAI.

For the simulated LAI, we first calculated the normalized LAI of each model referring to the normalization method of MODIS LAI, then calculated the arithmetic mean of the normalized LAI of each model to represent the normalized simulated LAI:

$$LAI^i_{Environmental\_normalized,year} = \frac{LAI^i_{Environmental,year}}{\overline{LAI^i_{Environmental}}}, \tag{2}$$

$$LAI_{Environmental\_normalized,year} = \sum_{i=1}^{n} LAI^i_{Environmental\_normalized,year} / n, \tag{3}$$

where $LAI_{Environmental\_normalized,year}$ is the normalized simulated LAI at a certain year acquired from S2 scenario from TRENDYv9 project. $LAI^i_{Environmental\_normalized,year}$ and $LAI^i_{Environmental,year}$ is the normalized and simulated LAI for model i (i = 1, 2, 3, 4, 5) at a certain year. $\overline{LAI^i_{Environmental}}$ is the multi-year average simulated LAI of model i.

2.3.2. Quantify the Relative Contribution of Multiple Factors to the LAI Trend

By integrating the normalized MODIS LAI and normalized simulated LAI, we explored the biological and physical pathways affecting Loess Plateau ecosystem structures. We hypothesized that the simulated results of the TRENDY project and MODIS observation data are accurate and we ignored the uncertainties, then the normalized simulated LAI calculated from the "S2" scenario of the TRENDY project can reflect the relative interannual

change in the terrestrial ecosystem under the influence of environmental change (e.g., climatic change, CO_2 fertilization, nitrogen deposition, etc.), and normalized MODIS LAI can capture the influences of both environmental change and human land-use management. Therefore, if the environmental signal was remoted from the MODIS LAI time series, the residuals can be attributed to the effects of human land-use management at a certain year ($LAI_{Human\_normalized,year}$), that is:

$$LAI_{Human\_Normalized,year} = LAI_{MODIS\_Normalized,year} - LAI_{Environmental\_normalized,year}, \quad (4)$$

The trends of $LAI_{MODIS\_normalized,year}$, $LAI_{Environmental\_normalized,year}$, and $LAI_{Human\_normalized,year}$ during the study period can be employed to represent the interannual change rates of actual LAI ($LAI_{MODIS\_normalized}$), environmental-induced LAI ($LAI_{Environmental\_normalized}$), and human-induced LAI ($LAI_{Human\_normalized}$), respectively. The least-square linear regression was used to determine the regression coefficients. A *P* value < 0.05 was considered significant. Additionally, we also evaluated the significance between the slopes of $LAI_{Environmental\_normalized}$ and $LAI_{Human\_normalized}$ changes from 2000 to 2019 by SPSS software. Notably, LAI variations that cannot be directly attributed to environmental change were assumed to be explained by the effects of human land-use management. Therefore, anthropogenic impacts can be both direct and indirect via synergy with environmental factors [36].

Furthermore, the scenarios "S1" and "S2" acquired from the TRENDY project were used to identify the impacts of CO_2 fertilization and climate change. The direct effect of CO_2 fertilization (CO_2 fertilization-induced LAI) was reflected in scenario "S1". The effect of climate change (climate-induced LAI) was regarded as the difference between scenarios "S2" and "S1". The simulation results of scenarios "S2" and "S1" were both normalized using the method described above.

A simple linear regression method was used to investigate trends in satellite-based LAI, that is LAI_{MODIS}, during the study period to reflect the actual vegetation change. A *P* value < 0.05 was considered significant. The simple linear regression method was also used to calculate the slopes of normalized LAI (e.g., $LAI_{MODIS\_normalized}$, $LAI_{Environmental\_normalized}$ and $LAI_{Human\_normalized}$). The ratios of $LAI_{Environmental\_normalized}$ slope to $LAI_{MODIS\_normalized}$ slope, and $LAI_{Human\_normalized}$ slope to $LAI_{MODIS\_normalized}$ slope represent the relative contributions of environmental factors and human land-use management to actual vegetation greening, respectively. Meanwhile, the ratios of the normalized CO_2 fertilization-induced LAI slope to $LAI_{Environmental\_normalized}$ slope, and normalized climate-induced LAI slope to $LAI_{Environmental\_normalized}$ slope represent the relative contributions of CO_2 fertilization and climate change to environmental-induced vegetation greening, respectively.

2.3.3. Statistical Methods

The spatial resolutions of satellite-based LAI, simulated LAI, and CRU meteorological data are so different that they cannot be directly compared at the grid scale. Therefore, we calculated the average LAI and meteorological values for the whole study area and each province, and then we separated the influence of human land-use management and environmental factors at the regional scale.

To investigate the response of interannual variation of LAI to climate change (i.e., temperature, precipitation, and download solar radiation), a partial correlation analysis method was carried out on the climate-induced LAI.

3. Results
3.1. Actual Vegetation Changes Based on LAI_{MODIS}

The LAI_{MODIS} on the Loess Plateau shows a gradient, with decreasing values from southeast to northwest (Figure 2). The LAI_{MODIS} values were greater than 4 m^2 m^{-2} in the southeastern Loess Plateau, mainly due to the abundant precipitation, and woodland was extensively distributed. Meanwhile, in the northwestern region, low annual precipitation limited vegetation growth, and the dominant vegetation cover was grassland, with

LAI$_{MODIS}$ generally below 0.5 m^2 m^{-2}. For the remaining regions, where farmland was widely distributed, the LAI$_{MODIS}$ ranged from 1 to 4 m^2 m^{-2}.

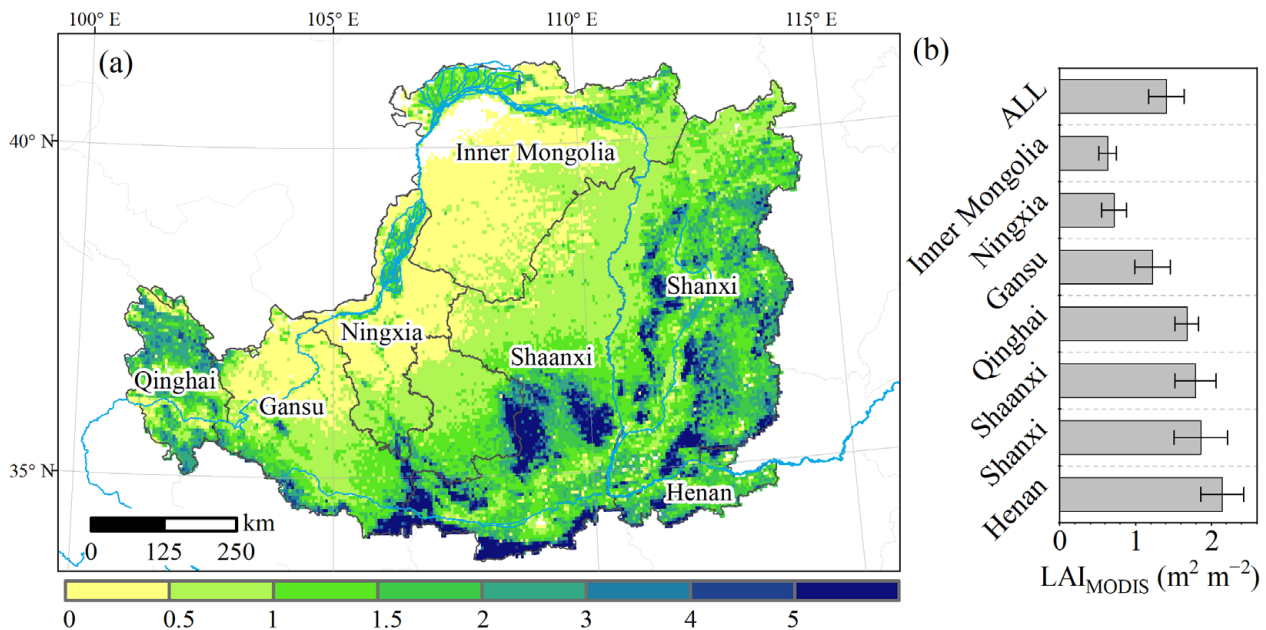**Figure 2.** (**a**) The spatial pattern and (**b**) average values for each province of MODIS LAI on the Loess Plateau.

The multiyear average LAI$_{MODIS}$ for the Loess Plateau was 1.40 $\pm$ 0.23 m^2 m^{-2} (mean $\pm$ standard deviation) during the study period (Figure 2b). The highest LAI$_{MODIS}$ occurred in Henan Province, with a value of 2.14 $\pm$ 0.28 m^2 m^{-2}, followed by Shanxi (1.86 $\pm$ 0.35 m^2 m^{-2}) and Shaanxi (1.79 $\pm$ 0.27 m^2 m^{-2}). Ningxia and Inner Mongolia had relatively low LAI$_{MODIS}$, with values of 0.71 $\pm$ 0.16 m^2 m^{-2} and 0.64 $\pm$ 0.12 m^2 m^{-2}, respectively, mainly due to the dry climate and low temperature. Moreover, LAI$_{MODIS}$ varied widely among biomes (Figure S1a). Woodland showed the highest average LAI$_{MODIS}$ (2.70 $\pm$ 0.06), which was more than twice that of farmland and grassland.

The LAI$_{MODIS}$ exhibited a significant positive trend ($P < 0.01$) across the study area between 2000 and 2019, where the slope $\pm$ standard errors were 0.037 $\pm$ 0.006 m^2 m^{-2} a^{-1}, and the change rate was 2.6% a^{-1} compared with the annual mean LAI$_{MODIS}$. The overall increasing trends of LAI$_{MODIS}$ were consistent for each province, and the positive trends were all significant at the 0.01 level (Figure 3b). The largest increase in LAI$_{MODIS}$ was in Shanxi, with an annual increase of 0.057 $\pm$ 0.007 m^2 m^{-2} a^{-1}, followed by Shaanxi (0.044 $\pm$ 0.005 m^2 m^{-2} a^{-1}), Henan (0.042 $\pm$ 0.009 m^2 m^{-2} a^{-1}), Gansu (0.036 $\pm$ 0.006 m^2 m^{-2} a^{-1}), Ningxia (0.024 $\pm$ 0.005 m^2 m^{-2} a^{-1}), and Qinghai (0.022 $\pm$ 0.006 m^2 m^{-2} a^{-1}). Inner Mongolia showed the lowest growth trend at 0.017 $\pm$ 0.004 m^2 m^{-2} a^{-1}. However, after normalizing the trends with the average LAI$_{MODIS}$ values, Ningxia exhibited the largest rate of increase at 3.36% per year, followed by Shanxi (3.05% a^{-1}); Qinghai showed the lowest relative increasing trend, with a value of 1.33% a^{-1} (Figure S2). Among the different biomes, woodland exhibited the highest increasing trend, with a value of 0.061 $\pm$ 0.009 m^2 m^{-2} a^{-1}, followed by farmland (0.038 $\pm$ 0.006 m^2 m^{-2} a^{-1}) and grassland (0.033 $\pm$ 0.005 m^2 m^{-2} a^{-1}) (Figure S1b).

The spatial heterogeneity of the interannual LAI$_{MODIS}$ variation was shown in Figure 3. More than 96% of the regions exhibited an upward trend in LAI$_{MODIS}$, and approximately 76% of the regions showed a significantly and positively rising trend. The LAI$_{MODIS}$ increased the most in the southeastern area of the study area (e.g., most parts of Shanxi, central Shaanxi, and southeastern Gansu), with an annual increase of more than 0.10 m^2 m^{-2} a^{-1}; moreover, a relatively low increase in growing season LAI$_{MODIS}$ occurred mainly on the

northwestern Loess Plateau, with annual increase values below $0.01 \, \text{m}^2 \, \text{m}^{-2} \, \text{a}^{-1}$. Additionally, about 4% of the study area showed a downward $\text{LAI}_{\text{MODIS}}$ trend, mainly distributed around cities such as Xi'an, Weinan, Baoji, Taiyuan, and Hohhot.
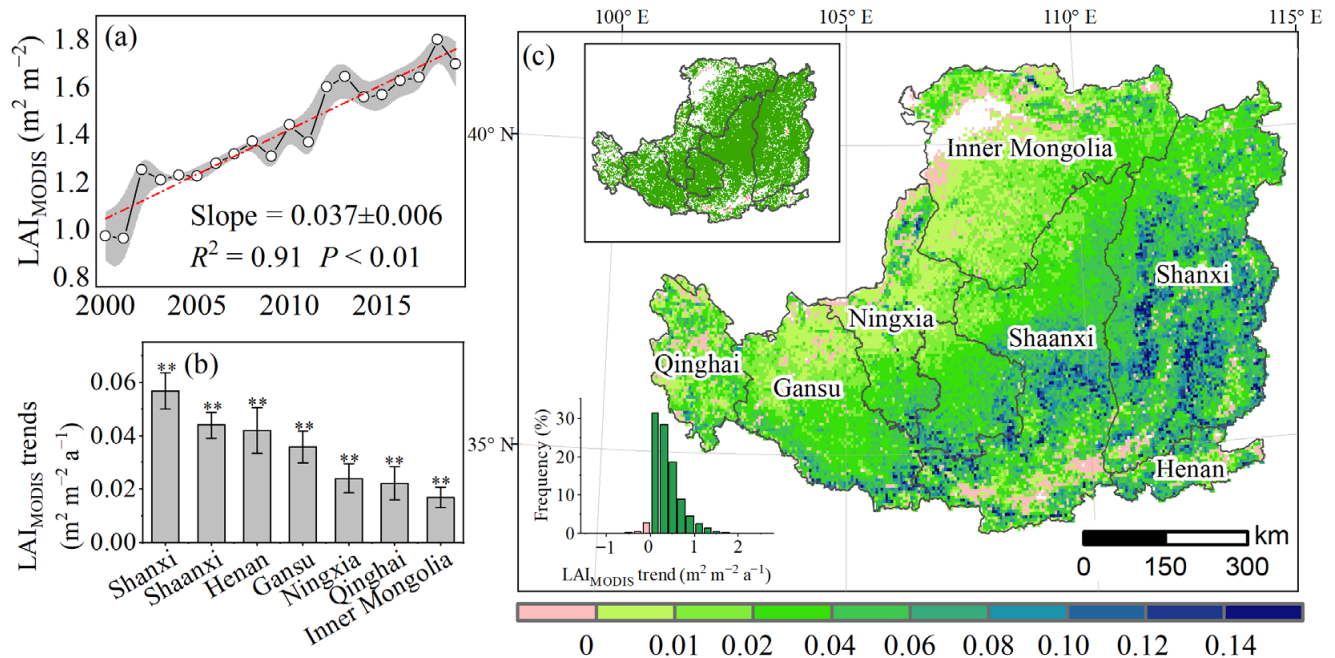

Figure 3. The interannual trend of $\text{LAI}_{\text{MODIS}}$ on the Loess Plateau During 2000–2019. (**a**) The interannual variations in $\text{LAI}_{\text{MODIS}}$ on the Loess Plateau; (**b**) the interannual variation in $\text{LAI}_{\text{MODIS}}$ for each province of the Loess Plateau (** represents $P < 0.01$); (**c**) spatial distribution of $\text{LAI}_{\text{MODIS}}$ trends. The inset map at the top-left corner shows the significant increasing (green) or decreasing trend (blue) in $\text{LAI}_{\text{MODIS}}$ during the study period; the inset graph at the bottom-left corner describes the frequency distribution of satellite-based $\text{LAI}_{\text{MODIS}}$ trends.

3.2. Influences of Natural and Human Factors on Vegetation Changes

Simulated results obtained from the scenario S2 of TRENDY project indicated vegetation changes under the influence of environmental factors (Figure 4). All models showed significant increases in the simulated LAIs due to the impact of environmental factors, but there were large differences in its magnitudes, with values between $0.007 \pm 0.006 \, \text{m}^2 \, \text{m}^{-2} \, \text{a}^{-1}$ for the ISAM model and 0.046 ± 0.022 for the LPX-Bern model (Figure 4b). Moreover, we found that the magnitudes of the multiyear average simulated LAIs also differed, with values between $1.25 \pm 0.14 \, \text{m}^2 \, \text{m}^{-2}$ for the ORCHIDEEv3 model and $3.853 \pm 0.46 \, \text{m}^2 \, \text{m}^{-2}$ for the LPX-Bern model (Figure 4a).

We identified the relative contributions of environmental factors and human land-use management to the actual vegetation change based on the normalized LAIs (Figure 5). The $\text{LAI}_{\text{MODIS\_normalized}}$ showed a distinct positive trend from 2000 to 2019 over the entire study area, with an increased value of 0.026 ± 0.005 ($P < 0.01$), indicating significant actual vegetation greening. $\text{LAI}_{\text{Human\_normalized}}$ showed a significant increasing trend, with a value of 0.014 ± 0.004 ($P < 0.01$), explaining approximately 54% of the greening trend; meanwhile, $\text{LAI}_{\text{Environmental\_normalized}}$ also showed a significantly positive trend, with a value of 0.012 ± 0.006 ($P < 0.01$), explaining 46% of the greening trend (Figure 5a). The results indicated that environmental factors and human land-use management explained 46% and 54% of the actual vegetation changes, respectively. Additionally, the comparison between slopes of $\text{LAI}_{\text{Environmental\_normalized}}$ and $\text{LAI}_{\text{Human\_normalized}}$ from 2000 to 2019 showed no statistically significant difference ($P > 0.05$), indicating that the impact of environmental changes and human land-use management may interact.
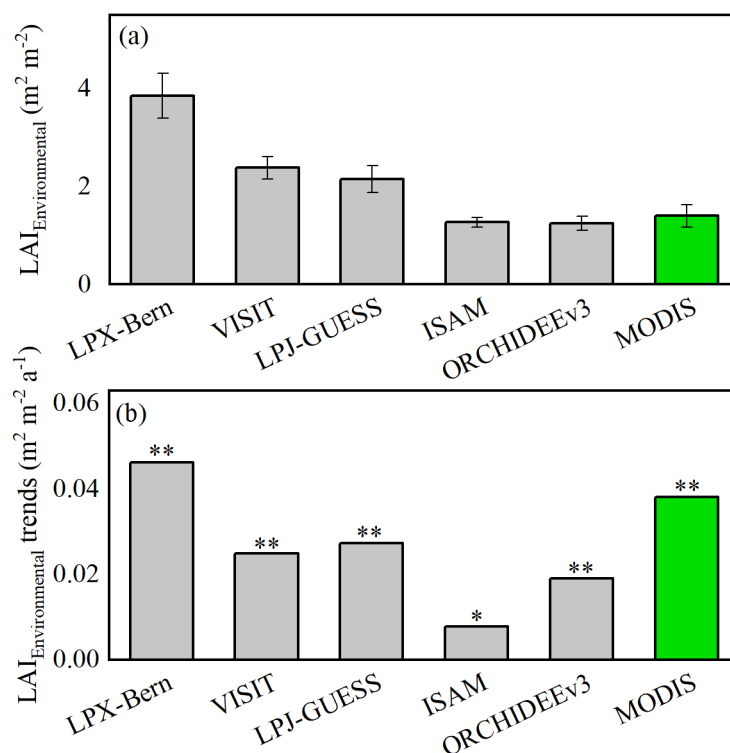
Figure 4. (**a**) Average environmental-induced LAIs based on the Scenario S2 from TRENDY project and (**b**) interannual trends of those LAIs in the Loess Plateau during the period between 2000 and 2019. * represents $P < 0.05$; ** represents $P < 0.01$.

For the different provinces (Figure 5b), human land-use management explained most of the vegetation greening trend, ahead of environmental changes in Gansu, Ningxia, Shaanxi, Shanxi, and Henan. Particularly in Gansu, Ningxia, and Shaanxi, the relative contribution of human land-use management exceeded 63%. Moreover, for Qinghai and Inner Mongolia, environmental change dominated the increasing trend of the actual vegetation conditions. In Qinghai, environmental change contributed to 80% of the actual vegetation increasing trend.

3.3. Effects of Different Environmental Factors on Vegetation Changes

Environmental change has markedly altered the dynamics of terrestrial vegetation. For all the study regions, CO_2 fertilization effects and nitrogen deposition explained 55% of the environmental change-driven greening trend from 2000 to 2019, while climate change explained 45% (Figure 6a). The influences of different environmental factors on vegetation growth exhibited large spatial heterogeneity. For the eastern Loess Plateau, CO_2 fertilization dominated the greening trend caused by environmental change, with the relative contributions of 74%, 61%, and 52% by Henan, Shanxi, and Shaanxi, respectively. For the western of study area, climate changes dominated the greening trend caused by environmental factors, and the relative contributions of Inner Mongolia, Ningxia, Gansu, and Qinghai were greater than 60%, which can be primarily ascribed to the dry climate in this area.
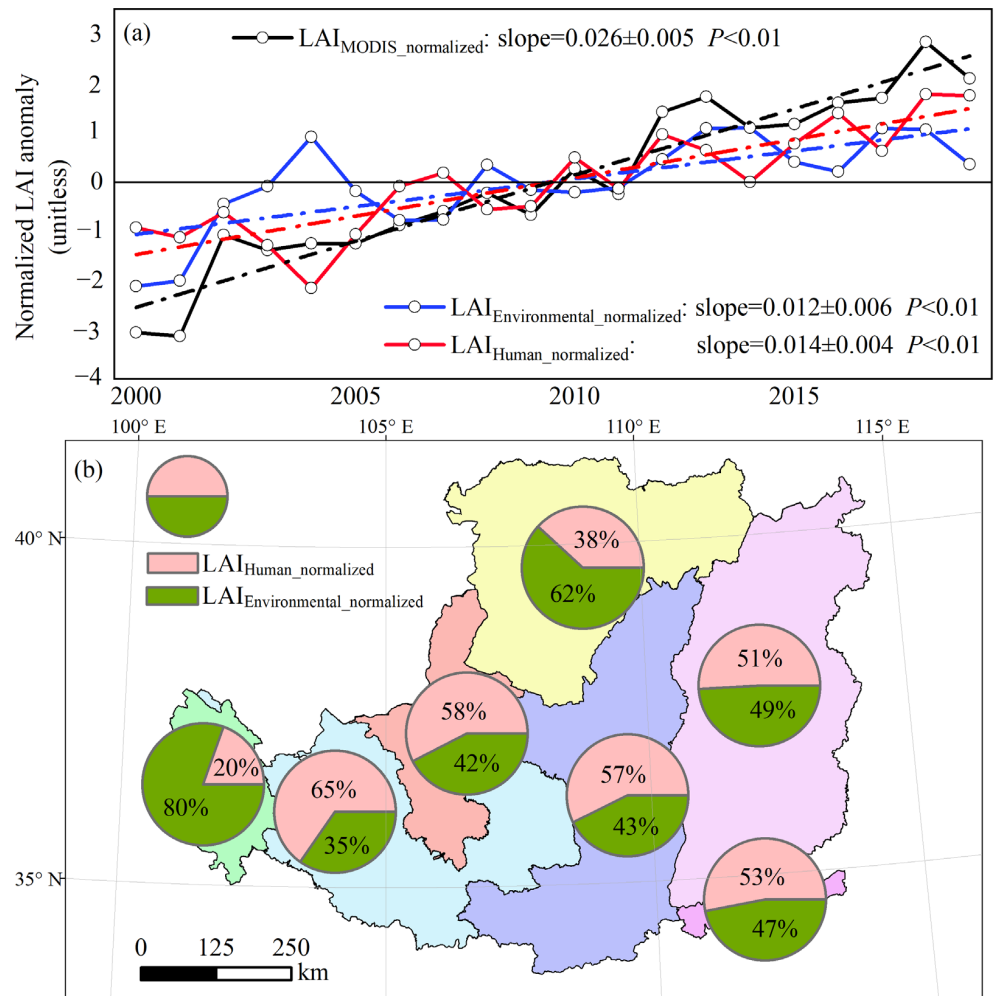
Figure 5. The influences of natural and anthropogenic factors on vegetation change in the Loess Plateau during 2000–2019. (**a**) The relative interannual trends of actual LAI (LAI$_{MODIS\_normalized}$), environmental change-induced LAI (LAI$_{Environmental\_normalized}$) and human land-use management-induced LAI (LAI$_{Human\_normalized}$). Anomalies were calculated as the difference between the normalized LAI for a given year and the average value during the study period. (**b**) The relative contribution of environmental change and human land-use management to the actual LAI trends for each province.

Furthermore, we investigated the influences of climatic variables on greening trends. Climate-induced LAI were significantly and positively correlated with solar radiation ($R = 0.75$) and precipitation ($R = 0.54$) across the whole study area. The correlations between climate-induced LAI and climatic variables varied across provinces (Figure 6b). Specifically, downscaled solar radiation dominated the interannual climate-induced LAI variation in Shanxi, Shaanxi, Henan, and Qinghai, which have relatively abundant precipitation or large areas with irrigation. Moreover, precipitation was the dominant driver in Inner Mongolia, Gansu, and Ningxia, which can be ascribed to the dry climate.
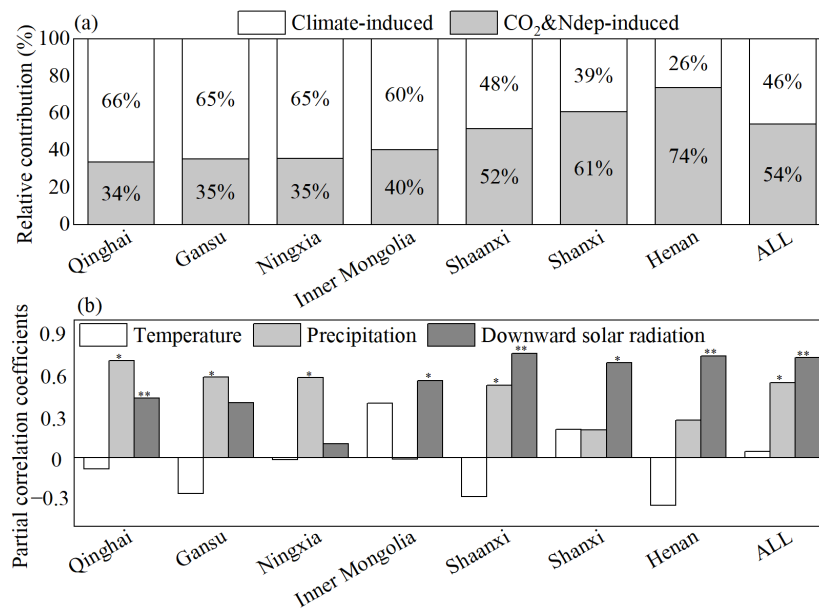
Figure 6. (**a**) Relative importance of climate change and CO_2 fertilization to environmental-induced LAI on the Loess Plateau from 2000 to 2019. (**b**) Partial correlation coefficients between climate-induced LAI and climate factors. * = $P < 0.05$ and ** = $P < 0.01$.

3.4. Relationship between Actual Vegetation Growth and Forest Area

The relationship between forest area and $LAI_{MODIS\_normalized}$ variations is shown in Figure 7. The changes in forest area were significantly and positively correlated with the $LAI_{MODIS\_normalized}$, with an explanatory value of 83% for the whole Loess Plateau, suggesting that the increase in forest area is a main underlying driver for the observed vegetation greening trend. Moreover, the relationships between forest area and $LAI_{MODIS\_normalized}$ were consistent among provinces, explaining more than 60% of the variability; in particular, for Ningxia, Shaanxi, and Shanxi, the relationship explained more than 96% of the variability in $LAI_{MODIS\_normalized}$ (Figure 7b). The interannual variability in forested areas, which was acquired from the 6th to the 9th national forest resource inventory, was consistent with the trend of $LAI_{MODIS\_normalized}$ in Shanxi and Shaanxi Provinces (Figure 7c,d).
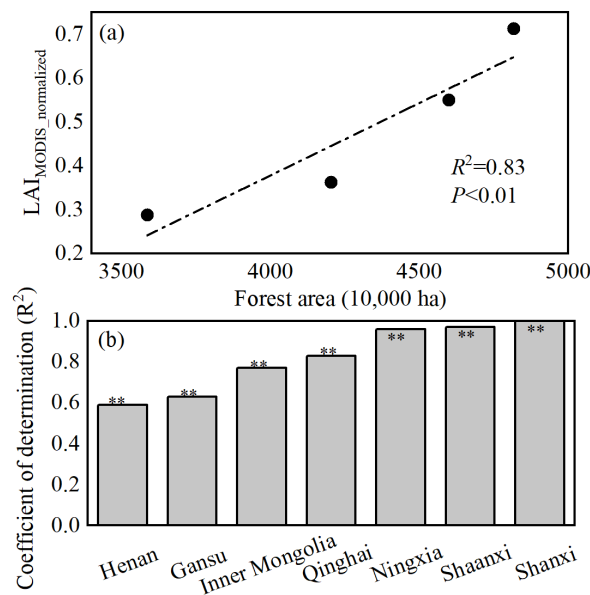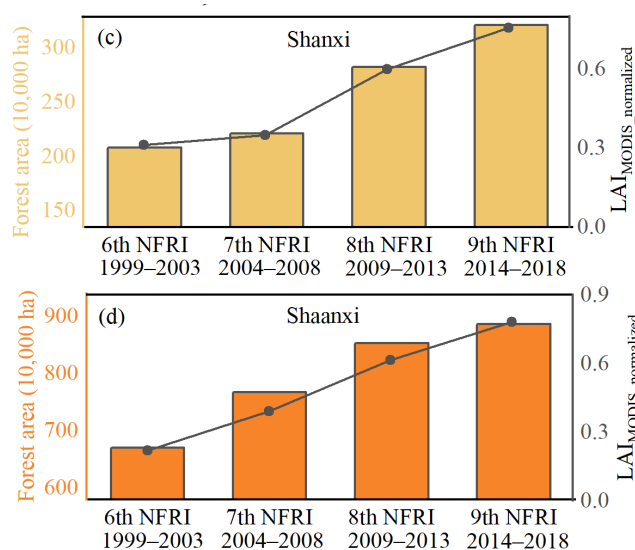

Figure 7. *Cont.*

Figure 7. Relationship between the $LAI_{MODIS\_normalized}$ trend and forest area for the (**a**) Loess Plateau, (**b**) different provinces, (**c**) Shanxi, and (**d**) Shaanxi. ** represents $P < 0.01$.

4. Discussion

4.1. Vegetation Greening Trend

Compared with other vegetation indexes, the leaf area index has a well-defined physical meaning in vegetation [1]. The leaf area index can be obtained from satellite products and is a simulated state variable in process-based models. Integrating satellite-based and simulated data from dynamic global vegetation models can attribute vegetation dynamics to different driving factors [2,13]. However, leaf area index values simulated by different models differed because of different assumptions and parameters [6], which led to uncertainties in the attribution analysis. Using simulation results from multiple models simultaneously can reduce the uncertainties [37]. Therefore, integration of remote sensing data with simulated results from multiple process-based models can improve the accuracy of attribution analysis.

Satellite-based data revealed increasing greenness in terrestrial ecosystems globally [1], with approximately 33% of the vegetated area turning green, and the leaf area increased by 2.3% per decade [14]. China, especially the Loess Plateau, showed a strong greening trend [26,27]. Specifically, approximately 76% of the regions exhibited a significant upward trend in LAI_{MODIS} since 2000 ($P < 0.05$), with a net increase rate of 27.1% in leaf area per decade, which was much higher than the global average. Meanwhile, there were spatiotemporal variations in greening across the study area. The LAI_{MODIS} increased significantly in the central and southeastern Loess Plateau and decreased around large cities. Thus, vegetation on the Loess Plateau generally exhibited greening trends, but some parts showed a brown trend.

4.2. Contributions of Multiple Factors to Vegetation Greening

Inferred human land-use management and environmental change jointly altered vegetation variations [1]. Intensive land use explained more than one-third of the observed greening trend at the global scale, with forests and croplands explaining 42% and 32% of the large-scale greening in China, respectively [14]. The Loess Plateau is one of the most noticeable greening areas in China, and human land-use management (such as ecological projects, cropland irrigation, population, etc.) has contributed 54% of the greening trends. The sharp increase in forest area caused by ecological projects such as Grain for Green has greatly promoted the vegetation greening trend [25,38]; the interannual trends of 5 years smoothing $LAI_{MODIS\_normalized}$ and forest coverage rate were similar (Figure 8). Cropland irrigation has also significantly contributed to the vegetation greening trend in the Loess

Plateau [27]. The middle and upper reaches of the Yellow River Basin (covering most area of the Loess Plateau) have exhibited a significant expansion of irrigated farmland, yet rainfed croplands were the dominant sources of irrigation expansion [39]. Additionally, GDP and population have also affected vegetation restoration (Figure 9). A large number of farm laborers have moved from the countryside to relatively lucrative city jobs, which has reduced human pressure on rural areas and promoted GDP [40,41]. Moreover, prohibiting practices damaging grasslands through fencing and grazing exclusion has helped protect ecologically important grassland zones [42].
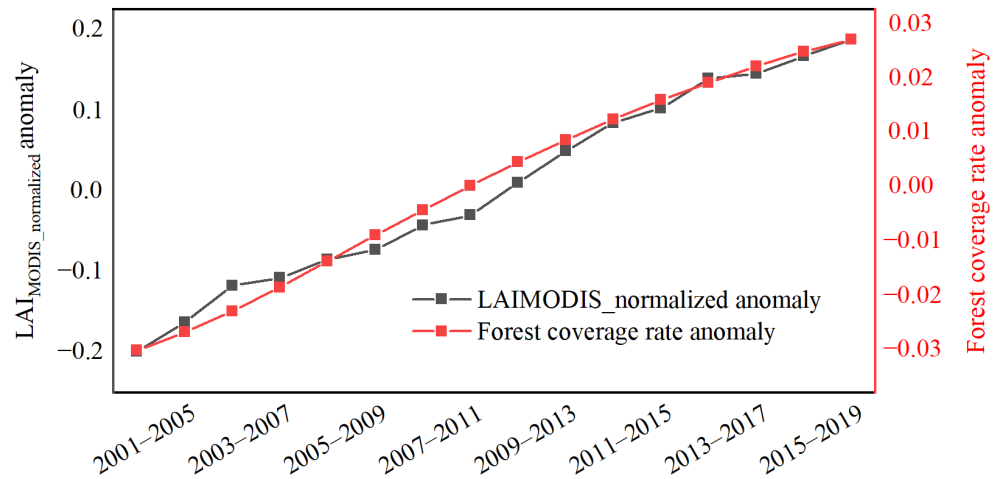

Figure 8. The interannual changes in the LAI$_{MODIS\_normalized}$ anomaly and forest coverage rate of the Loess Plateau from 2000 to 2019.
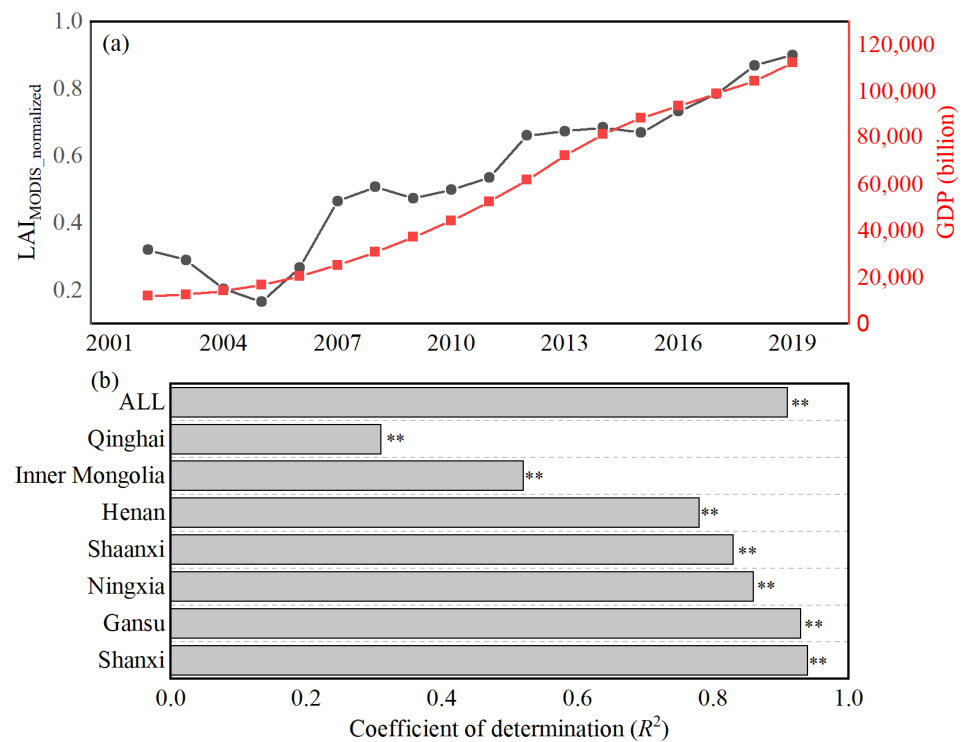

Figure 9. Relationship between LAI$_{MODIS\_normalized}$ and gross domestic product (GDP) since 2000 for (**a**) the Loess Plateau and (**b**) different provinces. ** represents $P < 0.01$.

Globally, the ensemble model with results simulated by the TRENDY project suggest that increasing atmospheric CO_2 accounts for approximately 70% of the vegetation greening

trend, while climate change only explains 8% [13]. Meanwhile, CO_2 fertilization accounts for 55% of the environmental-induced greening trend on the Loess Plateau, and climate change explains 45%. The Loess Plateau has a higher sensitivity to climate change compared with other areas on the global scale. Spatially, for the areas with relatively high leaf area (e.g., Henan, Shaanxi, and Shanxi), CO_2 fertilization is the major indirect driving factor for the greening trend because rising CO_2 concentrations can enhance photosynthesis [43] and extend the growth season [44]. Precipitation dominates vegetation variation in water-limited ecosystems (e.g., northwestern Loess Plateau) [9,28], and radiation is the main climate factor on the southeastern Loess Plateau. Additionally, rising CO_2 concentrations allow plants to operate at lower leaf stomata openings, which can conserve soil moisture and allow plants to grow a little longer into a drought cycle (e.g., Inner Mongolia, Ningxia, and Gansu) [9,45].

4.3. Limitations and Uncertainties

This study focused on trends in satellite and simulated data to quantify the impact of multiple drivers on vegetation change. However, whether the differences between satellite-observed and simulated LAIs can be directly attributed to human land-use management is debatable. This study was not a factorial experiment and there was an assumption made that MODIS LAI variation can be decomposed (TRENDY-based) environmental variation and residual variation that is attributed to human activities. The histograms of multi-year average $LAI_{MODIS\_normalized}$ and $LAI_{Environmental\_normalized}$ are compared in Figure 10. Both $LAI_{MODIS\_normalized}$ and $LAI_{Environmental\_normalized}$ were close to normally distributed, but the distribution of $LAI_{Environmental\_normalized}$ was more concentrated, the proportion of a normal distribution between 0.90 and 1.1 was 66%, while $LAI_{MODIS\_normalized}$ was 52%; when considering the normalized LAI above 1.2, the proportion of $LAI_{MODIS\_normalized}$ was higher than that of $LAI_{Environmental\_normalized}$, with values of 12% and 4%, respectively (Figure 10a). The distribution frequency of different models was similar (Figure 10b). Additionally, several studies have investigated key drivers of vegetation variations through combing satellite-observed and simulated data [2,13]. However, the over-sensitivity of models to atmospheric CO_2 has led to a satellite-derived productivity increase in less than half of the model-derived productivity rises during the past decades at the global scale [46], which implies a negative impact of anthropogenic activities if the trends are directly compared. For the Chinese terrestrial ecosystem, the average trend of satellite-observed LAI is greater than the trend of LAI estimated by models in 25 of 31 provinces, which can be partly explained by human activities, such as afforestation [37]. The research suggests that the comparison of satellite-observed and simulated LAI trends can partly explain the impacts of human land-use management in China.

Additionally, we must acknowledge that atmospheric CO_2 concentration and climate change are also significantly affected by human land-use management; therefore, anthropogenic factors might have greater influences than the value estimated in this study. Almost all the leaf areas simulated by process-based models exhibited uncertainties arising from model structure and parameter choices [37]. Therefore, the integrated simulated results from five models were used to separate the effects of different environmental factors on vegetation growth in this study. Additionally, the spatial resolutions mismatch between simulated and satellite-observed datasets increases the uncertainties; therefore, we conducted the analysis at the provincial level, which can help to reduce the impact of mismatch between spatial resolutions.
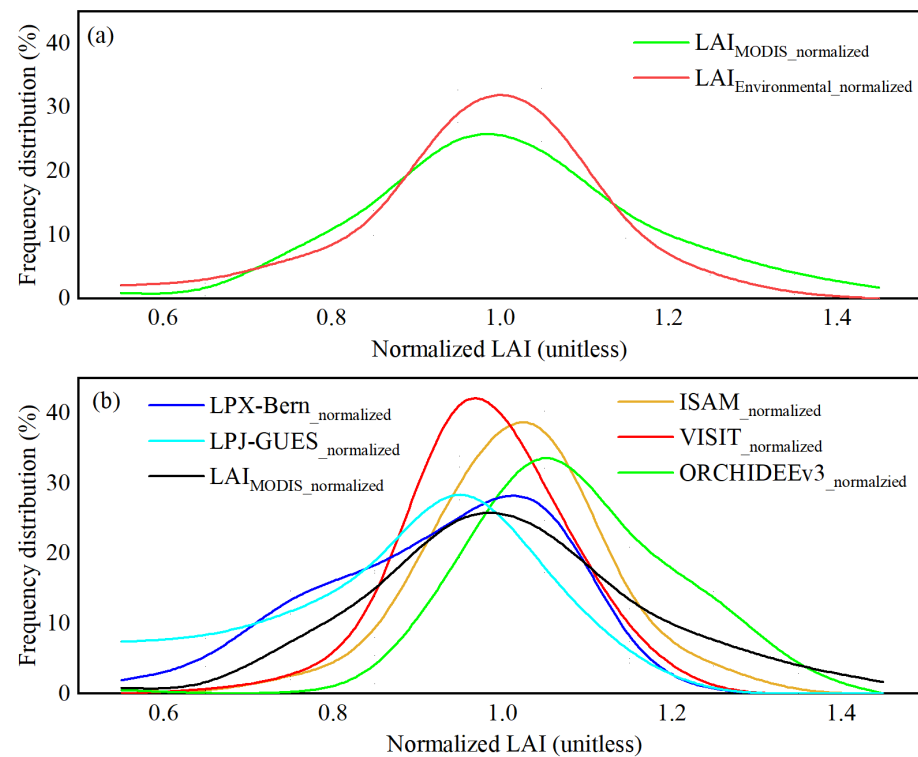
Figure 10. The frequency distribution of normalized LAI. (**a**) The frequency distribution of $LAI_{MODIS\_normalized}$ and $LAI_{Environmental\_normalized}$; (**b**) the frequency distribution of normalized MODIS LAI and normalized simulated LAI from models.

5. Conclusions

This study quantitatively assesses the drivers of vegetation growth in the Loess Plataea during the past decades through integrating satellite-derived LAI and simulated LAI from dynamic global vegetation models. The results showed that vegetation had an average annual increase of 0.037 ± 0.006 m^2 m^{-2} a^{-1} ($P < 0.01$). Human land-use management and environmental change jointly promoted vegetation restoration, with explanatory rates of 54% and 46%, respectively. CO_2 fertilization explained 55% of the greening trend caused by environmental change from 2000 to 2019, whereas climate change contributed 45%. Furthermore, solar radiation and precipitation dominated the climate-induced vegetation restoration ($P < 0.05$).

Author Contributions: Conceptualization, Z.N. and B.S.; Formal analysis, Z.N.; Resources, S.S., A.K.J. and N.V.; Software, Z.N.; Supervision, Z.N.; Writing—original draft, Z.N.; Writing—review and editing, H.H., P.Y., S.S., Y.Z., Y.W., A.K.J., N.V. and B.S. All authors have read and agreed to the published version of the manuscript.

Data Availability Statement: The MOD15A2H product was downloaded from https://lpdaac.usgs.gov/products/mod15a2hv006/, accessed on 1 July 2022; the TRENDY v9 project was downloaded from https://blogs.exeter.ac.uk/trendy/, accessed on 1 July 2022; the CRU historical meteorological dataset was downloaded from https://crudata.uea.ac.uk/cru/data/hrg/cru_ts_4.04/, accessed on 1 September 2022; the national forest resource inventory area was downloaded from http://www.

References

1. Piao, S.; Wang, X.; Park, T.; Chen, C.; Lian, X.; He, Y.; Bjerke, J.W.; Chen, A.; Ciais, P.; Tømmervik, H. Characteristics, drivers and feedbacks of global greening. *Nat. Rev. Earth Environ.* **2020**, *1*, 14–27. [CrossRef]

2. Mao, J.; Ribes, A.; Yan, B.; Shi, X.; Thornton, P.E.; Séférian, R.; Ciais, P.; Myneni, R.B.; Douville, H.; Piao, S.; et al. Human-induced greening of the northern extratropical land surface. *Nat. Clim. Chang.* **2016**, *6*, 959–963. [CrossRef]

3. Seddon, A.W.; Macias-Fauria, M.; Long, P.R.; Benz, D.; Willis, K.J. Sensitivity of global terrestrial ecosystems to climate variability. *Nature* **2016**, *531*, 229–232. [CrossRef] [PubMed]

4. Tong, X.; Brandt, M.; Yue, Y.; Horion, S.; Wang, K.; Keersmaecker, W.D.; Tian, F.; Schurgers, G.; Xiao, X.; Luo, Y.; et al. Increased vegetation growth and carbon stock in China karst via ecological engineering. *Nat. Sustain.* **2018**, *1*, 44–50. [CrossRef]

5. Lian, X.; Myneni, R.; Chapin Iii, F.; Callaghan, T.V.; Pinzon, J.; Tucker, C.J.; Zhu, Z.; Bi, J.; Ciais, P.; Tømmervik, H. Temperature and vegetation seasonality diminishment over northern lands. *Nat. Clim. Change* **2013**, *3*, 581–586.

6. Richardson, A.D.; Anderson, R.S.; Arain, M.A.; Barr, A.G.; Bohrer, G.; Chen, G.; Chen, J.M.; Ciais, P.; Davis, K.J.; Desai, A.R. Terrestrial biosphere models need better representation of vegetation phenology: Results from the N orth A merican C arbon P rogram S ite S ynthesis. *Glob. Change Biol.* **2012**, *18*, 566–584. [CrossRef]

7. Piao, S.; Nan, H.; Huntingford, C.; Ciais, P.; Friedlingstein, P.; Sitch, S.; Peng, S.; Ahlstrom, A.; Canadell, J.G.; Cong, N.; et al. Evidence for a weakening relationship between interannual temperature variability and northern vegetation activity. *Nat. Commun.* **2014**, *5*, 5018. [CrossRef]

8. Vickers, H.; Høgda, K.A.; Solbø, S.; Karlsen, S.R.; Tømmervik, H.; Aanes, R.; Hansen, B.B. Changes in greening in the high Arctic: Insights from a 30 year AVHRR max NDVI dataset for Svalbard. *Environ. Res. Lett.* **2016**, *11*, 105004. [CrossRef]

9. Fensholt, R.; Langanke, T.; Rasmussen, K.; Reenberg, A.; Prince, S.D.; Tucker, C.; Scholes, R.J.; Le, Q.B.; Bondeau, A.; Eastman, R. Greenness in semi-arid areas across the globe 1981–2007—An Earth Observing Satellite based analysis of trends and drivers. *Remote Sens. Environ.* **2012**, *121*, 144–158. [CrossRef]

10. Donohue, R.J.; McVICAR, T.R.; Roderick, M.L. Climate-related trends in Australian vegetation cover as inferred from satellite observations, 1981–2006. *Glob. Change Biol.* **2009**, *15*, 1025–1039. [CrossRef]

11. Keenan, T.F.; Hollinger, D.Y.; Bohrer, G.; Dragoni, D.; Munger, J.W.; Schmid, H.P.; Richardson, A.D. Increase in forest water-use efficiency as atmospheric carbon dioxide concentrations rise. *Nature* **2013**, *499*, 324–327. [CrossRef]

12. Yang, L.; Feng, Q.; Wen, X.; Barzegar, R.; Adamowski, J.F.; Zhu, M.; Yin, Z. Contributions of climate, elevated atmospheric CO_2 concentration and land surface changes to variation in water use efficiency in Northwest China. *Catena* **2022**, *213*, 106220. [CrossRef]

13. Zhu, Z.; Piao, S.; Myneni, R.B.; Huang, M.; Zeng, Z.; Canadell, J.G.; Ciais, P.; Sitch, S.; Friedlingstein, P.; Arneth, A.; et al. Greening of the Earth and its drivers. *Nat. Clim. Chang.* **2016**, *6*, 791–795. [CrossRef]

14. Chen, C.; Park, T.; Wang, X.H.; Piao, S.L.; Xu, B.D.; Chaturvedi, R.K.; Fuchs, R.; Brovkin, V.; Ciais, P.; Fensholt, R.; et al. China and India lead in greening of the world through land-use management. *Nat. Sustain.* **2019**, *2*, 122–129. [CrossRef]

15. Li, Y.; Liu, W.; Feng, Q.; Zhu, M.; Yang, L.; Zhang, J.; Yin, X. The role of land use change in affecting ecosystem services and the ecological security pattern of the Hexi Regions, Northwest China. *Sci. Total Environ.* **2023**, *855*, 158940. [CrossRef]

16. Yang, L.; Shen, F.; Zhang, L.; Cai, Y.; Yi, F.; Zhou, C. Quantifying influences of natural and anthropogenic factors on vegetation changes using structural equation modeling: A case study in Jiangsu Province, China. *J. Clean. Prod.* **2021**, *280*, 124330. [CrossRef]

17. Zhang, Y.; Wang, Q.; Wang, Z.; Yang, Y.; Li, J. Impact of human activities and climate change on the grassland dynamics under different regime policies in the Mongolian Plateau. *Sci. Total Environ.* **2020**, *698*, 134304. [CrossRef]

18. Jiang, L.; Bao, A.; Guo, H.; Ndayisaba, F. Vegetation dynamics and responses to climate change and human activities in Central Asia. *Sci. Total Environ.* **2017**, *599*, 967–980. [CrossRef]

19. Cao, W.; Wu, D.; Huang, L.; Pan, M.; Huhe, T. Determinizing the contributions of human activities and climate change on greening in the Beijing–Tianjin–Hebei Region, China. *Sci. Rep.* **2021**, *11*, 21201. [CrossRef]

20. Li, Y.; Liu, W.; Feng, Q.; Zhu, M.; Yang, L.; Zhang, J. Effects of land use and land cover change on soil organic carbon storage in the Hexi regions, Northwest China. *J. Environ. Manag.* **2022**, *312*, 114911. [CrossRef]

21. Zhang, Y.; Zhang, C.; Wang, Z.; Chen, Y.; Gang, C.; An, R.; Li, J. Vegetation dynamics and its driving forces from climate change and human activities in the Three-River Source Region, China from 1982 to 2012. *Sci. Total Environ.* **2016**, *563*, 210–220. [CrossRef] [PubMed]

22. Niu, Z.; He, H.; Zhu, G.; Ren, X.; Zhang, L.; Zhang, K.; Yu, G.; Ge, R.; Li, P.; Zeng, N. An increasing trend in the ratio of transpiration to total terrestrial evapotranspiration in China from 1982 to 2015 caused by greening and warming. *Agric. For. Meteorol.* **2019**, *279*, 107701. [CrossRef]

23. He, H.; Wang, S.; Zhang, L.; Wang, J.; Ren, X.; Zhou, L.; Piao, S.; Yan, H.; Ju, W.; Gu, F. Altered trends in carbon uptake in China's terrestrial ecosystems under the enhanced summer monsoon and warming hiatus. *Natl. Sci. Rev.* **2019**, *6*, 505–514. [CrossRef] [PubMed]

24. Liu, Z.; Wang, J.; Wang, X.; Wang, Y. Understanding the impacts of 'Grain for Green' land management practice on land greening dynamics over the Loess Plateau of China. *Land Use Policy* **2020**, *99*, 105084. [CrossRef]

25. Tian, F.; Liu, L.-Z.; Yang, J.-H.; Wu, J.-J. Vegetation greening in more than 94% of the Yellow River Basin (YRB) region in China during the 21st century caused jointly by warming and anthropogenic activities. *Ecol. Indic.* **2021**, *125*, 107479. [CrossRef]

26. Naeem, S.; Zhang, Y.; Zhang, X.; Tian, J.; Abbas, S.; Luo, L.; Meresa, H.K. Both climate and socioeconomic drivers contribute to vegetation greening of the Loess Plateau. *Sci. Bull* **2021**, *66*, 1160–1163. [CrossRef]

27. Kou, P.; Xu, Q.; Jin, Z.; Yunus, A.P.; Luo, X.; Liu, M. Complex anthropogenic interaction on vegetation greening in the Chinese Loess Plateau. *Sci. Total Environ.* **2021**, *778*, 146065. [CrossRef]

28. Nemani, R.R.; Keeling, C.D.; Hashimoto, H.; Jolly, W.M.; Piper, S.C.; Tucker, C.J.; Myneni, R.B.; Running, S.W. Climate-driven increases in global terrestrial net primary production from 1982 to 1999. *Science* **2003**, *300*, 1560–1563. [CrossRef]

29. Zheng, K.; Wei, J.Z.; Pei, J.Y.; Cheng, H.; Zhang, X.L.; Huang, F.Q.; Li, F.M.; Ye, J.S. Impacts of climate change and human activities on grassland vegetation variation in the Chinese Loess Plateau. *Sci. Total Environ.* **2019**, *660*, 236–244. [CrossRef]

30. Fu, B.; Wang, S.; Liu, Y.; Liu, J.; Liang, W.; Miao, C. Hydrogeomorphic ecosystem responses to natural and anthropogenic changes in the Loess Plateau of China. *Annu. Rev. Earth Planet. Sci.* **2017**, *45*, 223–243. [CrossRef]

31. Goldewijk, K.K. Estimating global land use change over the past 300 years: The HYDE database. *Glob. Biogeochem. Cycles* **2001**, *15*, 417–433. [CrossRef]

32. Yu, Z.; Ciais, P.; Piao, S.L.; Houghton, R.A.; Lu, C.Q.; Tian, H.Q.; Agathokleous, E.; Kattel, G.R.; Sitch, S.; Goll, D.; et al. Forest expansion dominates China's land carbon sink since 1980. *Nat. Commun.* **2022**, *13*, 5374. [CrossRef]

33. Harris, I.; Osborn, T.J.; Jones, P.; Lister, D. Version 4 of the CRU TS monthly high-resolution gridded multivariate climate dataset. *Sci. Data* **2020**, *7*, 109. [CrossRef]

34. Teckentrup, L.; De Kauwe, M.G.; Pitman, A.J.; Goll, D.S.; Haverd, V.; Jain, A.K.; Joetzjer, E.; Kato, E.; Lienert, S.; Lombardozzi, D. Assessing the representation of the Australian carbon cycle in global vegetation models. *Biogeosciences* **2021**, *18*, 5639–5668. [CrossRef]

35. Kobayashi, S.; Ota, Y.; Harada, Y.; Ebita, A.; Moriya, M.; Onoda, H.; Onogi, K.; Kamahori, H.; Kobayashi, C.; Endo, H. The JRA-55 reanalysis: General specifications and basic characteristics. *J. Meteorol. Soc. Jpn. Ser. II* **2015**, *93*, 5–48. [CrossRef]

36. Chen, Y.Z.; Feng, X.M.; Tian, H.Q.; Wu, X.T.; Gao, Z.; Feng, Y.; Piao, S.L.; Lv, N.; Pan, N.Q.; Fu, B.J. Accelerated increase in vegetation carbon sequestration in China after 2010: A turning point resulting from climate and human interaction. *Glob. Chang. Biol.* **2021**, *27*, 5848–5864. [CrossRef]

37. Piao, S.; Yin, G.; Tan, J.; Cheng, L.; Huang, M.; Li, Y.; Liu, R.; Mao, J.; Myneni, R.B.; Peng, S. Detection and attribution of vegetation greening trend in China over the last 30 years. *Glob. Change Biol.* **2015**, *21*, 1601–1609. [CrossRef]

38. Feng, X.; Fu, B.; Piao, S.; Wang, S.; Ciais, P.; Zeng, Z.; Lü, Y.; Zeng, Y.; Li, Y.; Jiang, X.; et al. Revegetation in China's Loess Plateau is approaching sustainable water resource limits. *Nat. Clim. Chang.* **2016**, *6*, 1019–1022. [CrossRef]

39. Bai, M.; Zhou, S.; Tang, T. A Reconstruction of Irrigated Cropland Extent in China from 2000 to 2019 Using the Synergy of Statistics and Satellite-Based Datasets. *Land* **2022**, *11*, 1686. [CrossRef]

40. Wei, J.-Z.; Zheng, K.; Zhang, F.; Fang, C.; Zhou, Y.-Y.; Li, X.-C.; Li, F.-M.; Ye, J.-S. Migration of rural residents to urban areas drives grassland vegetation increase in China's Loess Plateau. *Sustainability* **2019**, *11*, 6764. [CrossRef]

41. Li, W.; Li, X.; Tan, M.; Wang, Y. Influences of population pressure change on vegetation greenness in China's mountainous areas. *Ecol. Evol.* **2017**, *7*, 9041–9053. [CrossRef]

42. Wang, J.-J.; Jiang, Z.-D.; Xia, Z.-L. Grain-for-green policy and its achievements. In *Restoration and Development of the Degraded Loess Plateau, China*; Springer: Berlin/Heidelberg, Germany, 2014; pp. 137–147.

43. Farquhar, G.D.; Sharkey, T.D. Stomatal conductance and photosynthesis. *Annu. Rev. Plant Physiol.* **1982**, *33*, 317–345. [CrossRef]

44. Norby, R.J.; Zak, D.R. Ecological lessons from free-air CO_2 enrichment (FACE) experiments. *Annu. Rev. Ecol. Evol. Syst.* **2011**, *42*, 181–203. [CrossRef]

45. Ukkola, A.M.; Prentice, I.C.; Keenan, T.F.; Van Dijk, A.I.; Viney, N.R.; Myneni, R.B.; Bi, J. Reduced streamflow in water-stressed climates consistent with CO_2 effects on vegetation. *Nat. Clim. Chang.* **2016**, *6*, 75–78. [CrossRef]

46. Kolby Smith, W.; Reed, S.C.; Cleveland, C.C.; Ballantyne, A.P.; Anderegg, W.R.; Wieder, W.R.; Liu, Y.Y.; Running, S.W. Large divergence of satellite and Earth system model estimates of global terrestrial CO_2 fertilization. *Nat. Clim. Chang.* **2016**, *6*, 306–310. [CrossRef]